# Si Distribution in Silicoaluminophosphate Molecular Sieves with the LEV Topology: A Solid-State NMR Study

**Hye Ja Jung,[†] Chae-Ho Shin,[‡] and Suk Bong Hong*,[†]**

*Division of Chemical Engineering, Hanbat National University, Taejon 305-719, Korea, and Department of Chemical Engineering, Chungbuk National University, Chungbuk 361-763, Korea*

*Received: July 29, 2005; In Final Form: September 12, 2005*

The solid-state NMR evidence that Si atoms are not randomly distributed in microporous SAPO-35 materials with the LEV topology and their distribution is governed by the Si content in synthesis mixtures is presented. It is also shown that the extraction pattern of Si atoms from the two distinct tetrahedral sites of the SAPO-35 framework during the calcination step at elevated temperatures occurs in a nonrandom manner, which can be rationalized by considering the expected strain on each topologically distinct site. The overall results of this study reveal that, when the level of Si substitution in SAPO-35 materials is high enough to produce various heterogeneous Si environments other than Si(4Al) species having P atoms only as second-nearest T-atom neighbors, the oxide composition of the domain preferentially created is aluminosilicate rather than pure silica in nature.

## Introduction

Zeolites and related materials are a unique class of crystalline microporous solids that have a wide range of commercial applications as catalysts and separation media in the chemical industry. Many of the structures of already known zeolitic materials contain two or more crystallographically distinct tetrahedral sites (T-sites) characterized by different T−O bond lengths and T−O−T and O−T−O bond angles.[1] Thus, elucidating the manner in which various possible framework elements, e.g., Si, Al, P, Ga, Ge, Li, etc., are spatially distributed over the available T-sites in zeolites and molecular sieves is of fundamental importance in manipulating their physicochemical and catalytic properties at the molecular level.[2]

Since the initial discovery of a family of aluminophosphate ($AlPO_4$) molecular sieves by researchers at Union Carbide in the early 1980s,[3] over two dozen structures and three hundred compositions with frameworks incorporating one or more of 13 elements from the periodic table have been reported.[4] Unlike the case of silica frameworks,[5] however, few studies have focused on the understanding of the spatial distribution of heteroatoms other than Al and P in these $AlPO_4$−based molecular sieves. In particular, the question of the preference of Si atoms for particular T-sites in microporous silicoaluminophosphate (SAPO) materials remains to be answered. From a synthetic point of view, this appears to be due to the diverse nature of Si substitution in $AlPO_4$ frameworks that can be for P, an Al−P pair, or both of them, as well as to its generally low and narrow levels.[4b]

SAPO-35 is a member of the SAPO family and is isostructural with the natural zeolite levyne (LEV topology; see Figure 1) where only two distinct T-sites (i.e., $T_1$ in a double 6-ring (D6R) and $T_2$ in a single 6-ring (S6R) with multiplicities of 36:18, respectively) exist.[6] This has led us to consider SAPO-35 as a model structure of proving whether the location of Si atoms in microporous SAPO materials with multiple T-sites is spatially ordered. Here we present the $^{29}$Si MAS NMR evidence that substitution of Si atoms on the two distinct T-sites of the SAPO-35 framework during the crystallization process, as well as their extraction caused by calcination at elevated temperatures, occurs in a nonrandom manner. We also show that when the level of Si substitution in SAPO-35 materials is so high as to generate various heterogeneous Si environments, the resulting domains are aluminosilicate rather than pure-silica in nature.

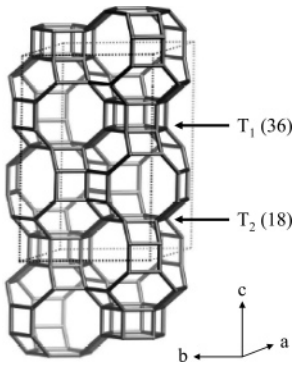


**Figure 1.** LEV framework showing two crystallographically distinct T-sites. Adapted from ref 6.

## Experimental Section

**Samples.** Four SAPO-35 samples with 3.0, 4.1, 5.8, and 9.4 Si atoms per unit cell, denoted as SAPO-35(I), SAPO-35(II), SAPO-35(III), and SAPO-35(IV), respectively, were synthesized using hexamethyleneimine (HMI) as an organic structure-directing agent (SDA) according to the procedure reported by Prakash et al.[7a] The overall oxide composition of the synthesis mixtures used in the crystallization of these four materials was $1.5HMI{\cdot}1.0Al_2O_3{\cdot}\ 1.0P_2O_5{\cdot}xSiO_2{\cdot}55H_2O$, where $x$ is 0.13, 0.25, 0.50, and 1.00. After stirring at room temperature for 24 h, the synthesis mixture was heated at 200 °C, without stirring under

* To whom correspondence should be addressed. Phone: +82-42-821-1549. Fax: +82-42-821-1593. E-mail: sbhong@hanbat.ac.kr

[†] Hanbat National University.

[‡] Chungbuk National University.

10.1021/jp054199j CCC: $30.25 
Published on Web 10/19/2005

autogenous pressure, for 24 or 48 h. The solid products were recovered by filtration, washed repeatedly with water, and then dried overnight at room temperature. As-made samples were calcined under flowing air at 550 °C for 12 h to obtain their organic-free proton form.

**Analytical Methods.** Powder X-ray diffraction (XRD) data were collected on a Rigaku 2500H diffractometer with Cu Kα radiation (40 kV and 200 mA). The samples were analyzed in the $2\theta$ range 3−50° with a step size of 0.01° and a count time of 2 s per step. Unit cell parameters in space group $R\bar{3}m$ were obtained by full-profile fitting of the powder XRD data using the program EXPO.[8] Elemental analysis for Si, Al, and Na was carried out by a Jarrell-Ash Polyscan 61E inductively coupled plasma spectrometer in combination with a Perkin-Elmer 5000 atomic absorption spectrophotometer. The C, H, and N contents of the samples were analyzed by using a Carlo Erba 1106 elemental organic analyzer. Thermogravimetric analyses (TGA) were performed in air on a TA Instruments SDT 2960 thermal analyzer, where the endothermic weight loss related to the desorption of water was further confirmed by differential thermal analyses (DTA) using the same analyzer. Crystal morphology and size were determined by a JEOL JSM-6300 scanning electron microscope (SEM). The Raman spectra were recorded on a Bruker RFA 106/S FT-Raman spectrometer equipped with an Nd:YAG laser operating at 1064 nm. The samples were exposed to a laser power of 100−250 mW at the spectral resolution of 4 $cm^{-1}$. Typically, 400−1600 scans were accumulated for obtaining the Raman spectra.

The $^1$H-$^{13}$C CP MAS NMR spectra at a spinning rate of 4.5 kHz were recorded on a Bruker Avance 500 spectrometer at a $^{13}$C frequency of 125.767 MHz with a $\pi/2$ rad pulse length of 5.0 $\mu$s, a contact time of 1 ms, and a recycle delay of 5 s. Approximately 1000 pulse transients were accumulated. The $^{29}$Si MAS NMR spectra at a spinning rate of 10.0 kHz were measured on the same spectrometer at a $^{29}$Si frequency of 99.352 MHz. The spectra were obtained with an acquisition of 7000−14000 pulse transients, which were repeated with a $\pi/2$ rad pulse length of 5.0 $\mu$s and a recycle delay of 30 or 60 s. Both $^{13}$C and $^{29}$Si chemical shifts are referenced to TMS. The $^{31}$P MAS NMR spectra at a spinning rate of 10.0 kHz were recorded at a $^{31}$P frequency of 202.450 MHz with a $\pi/2$ rad pulse length of 5.0 $\mu$s, a recycle delay of 30 s, and an acquisition of about 100 pulse transients. The $^{31}$P chemical shifts are referenced to a $H_3PO_4$ solution. The $^{27}$Al MAS NMR spectra at a spinning rate of 10.0 kHz were recorded at a $^{27}$Al frequency of 130.325 MHz. The spectra were obtained with an acquisition of ca. 1000 pulse transients, which were repeated with a $\pi/8$ rad pulse length of 1.2 $\mu$s and a recycle delay of 1 s. The $^{27}$Al chemical shifts are referenced to an $Al(H_2O)_6^{3+}$ solution. The spectra of dehydrated samples were collected after heating under vacuum to a residual pressure of $10^{-3}$ Torr at 250 °C for 24 h followed by packing into the rotors in a dry $N_2$ atmosphere. Spectral deconvolution and simulation were performed using the PeakFit curve-fitting program.

## Results and Discussion

Powder XRD experiments show that all SAPO-35 samples prepared in this study are highly crystalline and no reflections other than those from the LEV structure are observed, although some changes in relative X-ray peak intensities and positions for each sample are caused by calcination at 550 °C to remove the occluded SDAs followed by exposure to ambient air (Supporting Information Figure 1S). SEM photographs reveal that the four SAPO-35 samples appear typically as overlapped rhombohedra of 30−40 $\mu$m in diameter, while much more rounded crystallites are observed for the sample with a higher Si content (Supporting Information Figure 2S). The chemical composition data of their as-made form in Table 1 show that the Si content of each product increases with increasing the value for its synthesis mixture. A very close match between the amount of Al and the sum of P and Si atoms observed for SAPO-35(I) and SAPO-35(II) indicates that the Si atoms in these two SAPO-35 samples substitute for framework P sites only. However, there is a considerable imbalance between the amount of Al and the sum of P and Si atoms for the other two materials with higher Si contents, suggesting that the Si substitution pattern in SAPO-35(III) and SAPO-35(IV) is more complicated. This could perhaps explain the lack of a linear relationship between the number of Si atoms per unit cell of as-made SAPO-35 samples prepared here and their unit cell volume (Table 1).

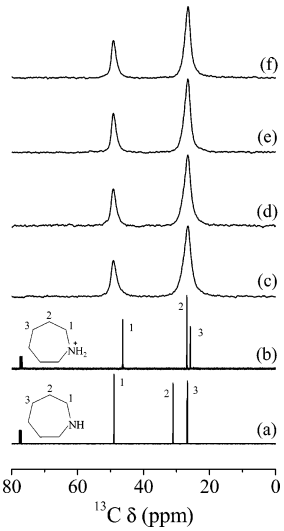


**Figure 2.** $^{13}$C NMR spectra of organic SDA, hexamethyleneimine (HMI): $^{13}$C NMR of (a) HMI and (b) protonated HMI ($HMI{\cdot}H^+$) in $CDCl_3$ solution and $^1$H-$^{13}$C CP MAS NMR of as-made (c) SAPO-35(I), (d) SAPO-35(II), (e) SAPO-35(III), and (f) SAPO-35(IV).

Figure 2 shows the $^1$H-$^{13}$C CP MAS NMR spectra of the four SAPO-35 samples with different Si contents in their as-made form, together with the liquid $^{13}$C NMR spectra of HMI and its protonated form (i.e., $HMI{\cdot}H^+$) in $CDCl_3$ solution, prepared by adding dilute HCl to HMI. As seen in Figure 2, the spectra of all as-made SAPO-35 materials are characterized by two $^{13}$C NMR lines at 26.5 and 49.1 ppm, suggesting that the variation in Si content has no effect on the $^{13}$C chemical shift of the occluded organic SDA. We note that while the chemical shift of their low-field $^{13}$C NMR resonance is essentially the same as that (49.4 ppm) of the first methylene carbon resonance observed for neutral HMI, the high-field line is close to the second methylene carbon resonance (27.2 ppm) of protonated HMI or the third methylene carbon resonance (27.1 ppm) of unprotonated HMI. However, this cannot be rationalized by simply considering the presence of a mixture of HMI and $HMI{\cdot}H^+$ residing in the same environment. In fact, if both species were present, the second methylene carbon resonance of HMI and the first methylene carbon resonance of $HMI{\cdot}H^+$ should appear around 31 and 46 ppm in the spectra of our as-made SAPO-35 samples, respectively. From the $^1$H-$^{13}$C CP MAS NMR spectra in Figure 2, therefore, we were not able to unambiguously confirm whether HMI is located as the protonated form inside the SAPO-35 pores.

To further address this issue, we performed Raman measurements on all SAPO-35 samples prepared here, as well as on

**TABLE 1: Physical Data for SAPO-35 Materials Prepared in This Study**

| sample | unit cell composition[a,b] | atomic Si fraction | unit cell parameters and volume | | | water content[b,c] | |
|---|---|---|---|---|---|---|---|
| | | | *a*, Å | *c*, Å | *V*, Å$^3$ | wt % | no. of molecules/ LEV cage |
| SAPO-35(I) | $3.1(HMI{\cdot}H^+OH^-){\cdot}3.0HMI{\cdot}H^+(Al_{27.0}P_{24.0}Si_{3.0})O_{108}{\cdot}7.1H_2O$ | 0.056 | 13.254 | 22.287 | 3390.5 | 25.7 | 7.8 |
| SAPO-35(II) | $2.4(HMI{\cdot}H^+OH^-){\cdot}4.1HMI{\cdot}H^+(Al_{27.0}P_{22.9}Si_{4.1})O_{108}{\cdot}7.6H_2O$ | 0.076 | 13.225 | 22.298 | 3377.7 | 29.1 | 8.9 |
| SAPO-35(III) | $3.0(HMI{\cdot}H^+OH^-){\cdot}3.6HMI{\cdot}H^+(Al_{25.9}P_{22.3}Si_{5.8})O_{108}{\cdot}8.2H_2O$ | 0.107 | 13.234 | 22.270 | 3378.0 | 29.3 | 8.9 |
| SAPO-35(IV) | $1.6(HMI{\cdot}H^+OH^-){\cdot}5.4HMI{\cdot}H^+(Al_{25.0}P_{19.6}Si_{9.4})O_{108}{\cdot}8.7H_2O$ | 0.174 | 13.255 | 22.312 | 3394.6 | 25.3 | 7.7 |

[a] Determined by elemental analysis except the water content. $HMI{\cdot}H^+$ is protonated HMI, and $OH^-$ has been introduced to make the as-made SAPO-35 samples electrically neutral. The number ($n$) per unit cell of $HMI{\cdot}H^+$ ions balancing the framework negative charges was calculated using the following simple equation: $n = n_{Al} - n_P$, where $n_{Al}$ and $n_P$ are the numbers per unit cell of Al and P atoms, respectively. [b] The water content of each sample was calculated from the endothermic weight loss appearing at temperatures below 250 °C in the TGA/DTA curves. [c] Measured on the samples that were first calcined under flowing air at 550 °C for 12 h and then exposed to ambient air at room temperature for 7 days.

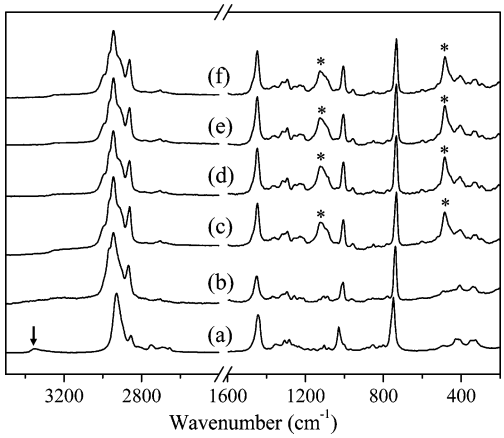


**Figure 3.** Raman spectra in the 200−3500 cm$^{-1}$ region of 0.5 M aqueous solution of (a) HMI and (b) protonated HMI, as well as of as-made (c) SAPO-35(I), (d) SAPO-35(II), (e) SAPO-35(III), and (f) SAPO-35(IV). The N−H stretching mode of neutral HMI is marked with an arrow, and the structural Raman bands of SAPO-35 are indicated by asterisks.

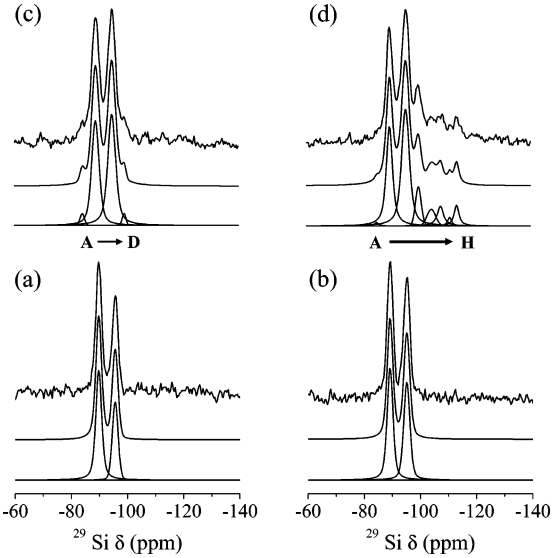


**Figure 4.** $^{29}$Si MAS NMR spectra of as-made (a) SAPO-35(I), (b) SAPO-35(II), (c) SAPO-35(III), and (d) SAPO-35(IV): experimental (top); simulated (middle); deconvoluted components (bottom). The deconvoluted $^{29}$Si NMR components for these four materials are denoted (from left to right) as lines A−H.

HMI and HMI:HCl. The Raman spectra in Figure 3 reveal that HMI not only remains intact inside the SAPO-35 pores, but also exhibits noticeable changes in the intensity and/or position of its specific Raman vibrational modes. While neutral HMI exhibits a broad asymmetric band around 3350 cm$^{-1}$ assigned to the N−H stretching mode,[9] neither protonated HMI nor SAPO-35 materials prepared here give this band. As seen in Figure 3, in addition, the Bohlmann bands[10] appearing in the 2700−2830 cm$^{-1}$ region whose intensities depend mainly on the presence of a lone pair on the nitrogen adjacent to the $CH_2$ group are significantly weaker for as-made SAPO-35 samples than for neutral HMI. These results clearly show that the organic SDA molecules trapped within the SAPO-35 pores exist as their protonated form, since there is no longer any lone pair on the nitrogen atom. Unlike protonated HMI, on the other hand, all as-made SAPO-35 samples prepared here show signs of four components in the 2900−3000 cm$^{-1}$ region, assignable to asymmetric $CH_2$ vibrations, which can be attributed primarily to host−guest interactions occurring between the SAPO-35 framework and the occluded organic species. Since the chemical composition data in Table 1 indicate that each of the hepta-decahedral [$4^9 6^5 8^3$] LEV cages of the four SAPO-35 samples, on an average, contains 1.0−1.2 HMI molecules in the protonated form, the guest−guest (i.e., HMI−HMI) interactions are not likely responsible for the observed splitting of $CH_2$ vibrations.

Figure 4 shows the $^{29}$Si MAS NMR spectra of a series of as-made SAPO-35 samples, together with the simulated spectra and their deconvoluted components. All the spectra are dominated by two prominent $^{29}$Si NMR resonances at −89.5 ± 0.3 and −95.4 ± 0.2 ppm. When using the equation of Ramdas and Klinowski,[11] the average Si−O−Al angles for the two $^{29}$Si lines from SAPO-35(I) were calculated to be 149.0 and 161.8°, respectively. These values are in reasonable agreement with the average $T_1$−O−T and $T_2$−O−T angles (148.5 and 155.5°, respectively) derived from the Rietveld refinement of the synchrotron powder XRD data for an as-made pure-silica levyne obtained in the presence of *N*-methylquinuclidinium ions,[12] despite the notable difference in framework compositions for the two materials compared here. Thus, the two tetrahedral $^{29}$Si NMR resonances appearing around −89 and −95 ppm in Figure 4 can be assigned to Si atoms in sites $T_1$ and $T_2$ with multiplicities of 36:18 of the SAPO-35 framework, i.e., $Si_1$-(4Al) and $Si_2$(4Al) in the D6R and S6R, respectively.[6] Figure 4 also shows that the $^{29}$Si MAS NMR spectra of SAPO-35(I) and SAPO-35(II) contain these two lines only, which is substantially different from the spectral feature of the samples with higher Si contents. This again confirms that the Si atoms in SAPO-35 samples with low Si contents substitute only for a portion of P atoms. The results from curve deconvolution of the $^{29}$Si MAS NMR spectra in Figure 4 are summarized in Table 2. It can be seen that the relative intensity ratios of the two tetrahedral components from SAPO-35(I) and SAPO-35(II) are considerably smaller than the ideal value (2:1) expected for the statistical distribution of Si atoms over the two sites $T_1$ and $T_2$ of the LEV framework. In particular, a much smaller value (1.1:1) distribution was calculated for the latter sample with a slightly

**TABLE 2: Chemical Shifts, Relative Intensities, and Assignments of the $^{29}$Si MAS NMR Resonances of a Series of As-Made SAPO-35 Materials with Different Si Contents**

| | $^{29}$Si $\delta_{obs}$,[b] ppm from TMS | | | | | | | | | | | |
|---|---|---|---|---|---|---|---|---|---|---|---|---|
| | SAPO-35(I) | | | SAPO-35(II) | | | SAPO-35(III) | | | SAPO-35(IV) | | |
| line[a] | $\delta$ (ppm) | $I$ (%) | assignment[c] | $\delta$ (ppm) | $I$ (%) | assignment[c] | $\delta$ (ppm) | $I$ (%) | assignment[c,d] | $\delta$ (ppm) | $I$ (%) | assignments[c,d] |
| A | | | | | | | −84.4 | 2.4 | $Si_1$(4Al) | −85.2 | 0.8 | $Si_1$(4Al) |
| B | −89.8 | 63.0 | $Si_1$(4Al)[9P] | −89.2 | 51.5 | $Si_1$(4Al)[9P] | −89.2 | 43.0 | $Si_1$(4Al)[9P] + $Si_1$(3Al) + $Si_2$(4Al) | −89.8 | 30.2 | $Si_1$(4Al)[9P] + $Si_1$(3Al) + $Si_2$(4Al) |
| C | −95.6 | 37.0 | $Si_2$(4Al)[10P] | −95.2 | 48.5 | $Si_2$(4Al)[10P] | −95.2 | 50.6 | $Si_2$(4Al)[10P] + $Si_1$(2Al) + $Si_2$(3Al) | −95.5 | 42.2 | $Si_2$(4Al)[10P] + $Si_1$(2Al) + $Si_2$(3Al) |
| D | | | | | | | −99.4 | 4.0 | $Si_1$(1Al) + $Si_2$(2Al) | −100.0 | 8.1 | $Si_1$(1Al) + $Si_2$(2Al) |
| E | | | | | | | | | | −104.7 | 5.1 | -[e] |
| F | | | | | | | | | | −107.9 | 6.5 | $Si_1$(0Al) + $Si_2$(1Al) |
| G | | | | | | | | | | −111.2 | 1.7 | -[e] |
| H | | | | | | | | | | −113.6 | 5.4 | $Si_2$(0Al) |
| $I_B/I_C$ | 1.70 | | | 1.06 | | | 0.85 | | | 0.72 | | |

[a] The same as the identification labels in Figure 4. [b] Observed chemical shifts from the deconvolution of the experimental spectra. [c] The assignments of the $^{29}$Si MAS NMR lines from Si atoms in the silicoaluminophosphate (SAPO) region of each sample are made based on comparison of the observed chemical shifts and the predicted chemical shifts from the reported average T−O−T angles for the two crystallographically distinct T-sites in an as-made pure-silica levyne prepared with *N*-methylquinuclidine ions[12] using the equation of Ramdas and Klinowski.[11] The numbers of P atoms in the second tetrahedral coordination sphere of the two distinct Si sites in the SAPO region are given in square brackets to distinguish from various Si environments in the aluminosilicate (AS) domain. [d] The assignments of the $^{29}$Si NMR resonances from Si atoms in the AS domain are done in a manner similar to those for Si in the SAPO region. For further details, see the text. [e] Not assigned.

higher Si content. This clearly shows that preferential substitution of Si into the low-multiplicity site with a larger T−O−T angle occurs during the crystallization process and its extent differs according to the Si content in SAPO-35 synthesis mixtures, which is essentially the same as the trend observed for the distribution of Al atoms in some aluminosilicate zeolites with multiple T-sites.[2,13] In the LEV topology, three O−T−O bonds of the high-multiplicity site are constrained within four rings, while in the low-multiplicity site only two O−T−O bonds are in such a situation.[6] Since strain on $T_1$ is larger than on $T_2$, it is not difficult to expect that the stability of secondary building units involving four rings is increased when some of P atoms with a formal oxidation state of +5 in the latter than in the former are substituted by Si, the less electronegative element with a lower oxidation state and a larger volume. To date, there are two published $^{29}$Si NMR spectra of SAPO-35 in which two prominent resonances are observed around −89 and −95 ppm,[7] as shown also here. Due to the poor spectral resolution or the use of the cross-polarization technique in $^{29}$Si MAS NMR measurements, however, no information on the intensity ratio of the two $^{29}$Si resonances has been available.

As seen in Figure 4, on the other hand, the $^{29}$Si MAS NMR spectrum of SAPO-35(III) is characterized by two additional low-intensity shoulders at −84.4 and −99.4 ppm, in addition to the two main resonances at −89.2 and −95.2 ppm, reflecting the presence of more than one type of oxide compositions of regions in this SAPO-35 sample. Given the absence of any noticeable resonance in the chemical shift region higher than −100 ppm, however, it is clear that there is no formation of pure-silica islands. According to the theoretical work by Barthomeuf,[14] the maximum Si fraction in the SAPO-35 framework, where all the Si atoms are isolated and hence reside in a single, homogeneous environment of Si(4Al) surrounded by P atoms only as second-nearest T-atom neighbors, was calculated to be 0.102 based on the topological density approach. Since this value is slightly lower than the Si fraction (0.107) in SAPO-35(III) obtained from elemental analysis, a portion of framework Si atoms in this SAPO-35 sample appears to be no longer isolated. When neglecting the presence of crystallographically distinct T-sites, the $^{29}$Si MAS NMR spectrum of a given aluminosilicate zeolite may consist of one to five lines corresponding to the five Si($n$Al) environments with $n = 0-4$ in the framework surrounded by Si atoms only as second-nearest neighbors due to the so-called Loewenstein's rule. With increasing the number ($n$) of Al atoms in the first tetrahedral coordination sphere of the Si atom, the $^{29}$Si NMR lines are systematically shifted to low field, where each Al substitution leads to a shift contribution of 5−6 ppm, and hence the Si(4Al) resonance falls normally into the chemical shift range −80 to −90 ppm from TMS, depending on the actual zeolite structure.[15] As described earlier, no evidence for the presence of more than one phase in all SAPO-35 samples prepared here was found. Since the $^{29}$Si chemical shift of $Si_1$(4Al) species with a smaller average T−O−T angle in the LEV framework should be lower than that of $Si_2$(4Al) species with a larger T−O−T angle,[11] the weak shoulder appearing at −84.4 ppm in the spectrum of SAPO-35(III) can be reasonably assigned to $Si_1$(4Al) species, indicating the formation of aluminosilicate (AS) domains in this SAPO-35 sample. The observed difference (∼5 ppm) in chemical shift between this lowest-field shoulder and the prominent resonance at −89.5 ± 0.3 ppm, unequivocally assigned to $Si_1$(4Al) species in the silicoaluminophosphate (SAPO) region as described above, suggests that the shift effect of having the less electronegative Si compared to P as the second-nearest neighbor in the SAPO-35 framework may be comparable in magnitude to that (∼6 ppm) due to T-site nonequivalence in its SAPO region. If such is the case, the low-intensity resonance around −89 ppm should then be attributed to the overlap of signals for $Si_1$(3Al) and $Si_2$(4Al) in the AS domain with the main signal for $Si_1$(4Al) in the SAPO region. As given in Table 2, in addition, a similar assignment can be made for the resonance appearing around −95 ppm in the $^{29}$Si MAS NMR spectrum of SAPO-35(III).

The most complicated $^{29}$Si MAS NMR spectrum among the spectra in Figure 4 was obtained from SAPO-35(IV), as expected from its Si fraction (0.174) being considerably higher than the maximum content (0.107) of isolated Si atoms in the SAPO-35 framework. Unlike in the spectrum of SAPO-35(III),

the shoulder around −85 ppm assigned to $Si_1(4Al)$ species in AS domains is barely detectable. However, the relative intensity of the resonance around −100 ppm due to the sum of $Si_1(1Al)$ and $Si_2(2Al)$ species was found to be considerably larger than the corresponding resonance observed for SAPO-35(III). It is thus clear that the domains in SAPO-35(IV), where no P atoms exist any longer, are more siliceous than those in SAPO-35-(III). This can be further supported by the fact that the $^{29}$Si MAS NMR spectrum of SAPO-35(IV) also shows signs of at least four deconvoluted components in the chemical shift region higher than −100 ppm, although the signal-to-noise ratio in this region is still poor even after an acquisition time of 5 days. Assuming that the $^{29}$Si chemical shift differences caused by T-site nonequivalence in the AS and SAPO domains of this SAPO-35 sample are similar to each other, the use of the shift change (5.6 ppm) reported by Ramdas and Klinowski[11] against each Al substitution in the first tetrahedral coordination sphere of Si atoms in the AS region allows us to tentatively assign some of these high-field deconvoluted components to the structural species listed in Table 2. Based upon the approach given above, however, we were not able to reasonably assign the two weak-intensity lines appearing around −105 and −111 ppm, although they could be related to the presence of connectivity defects (Si−$O^-$ or Si−OH groups) and amorphous silica, respectively.[15,16] An alternative explanation is the heterogeneity in second-nearest T-atom neighbors of the Si atoms positioned at the border between the AS and SAPO domains, because the chemical shift effect of having the less electronegative Si instead of P as the second-nearest neighbor in the SAPO-35 framework are significant as described above. Regardless of the exact assignments of these two resonances, the fact that the relative intensity of the highest-field resonance assignable to $Si_2(0Al)$ species is lower than that of the resonance appearing around −100 or −108 ppm suggests that there is no significant pure-silica island formation.

Currently, it is not possible to quantitatively estimate the relative Si populations over the two distinct T-sites in AS and SAPO domains and their proportions in the SAPO-35(III) and SAPO-35(IV) crystals from the $^{29}$Si MAS NMR data because many of the observed resonances originate from more than one single Si environment. However, the curve deconvolution results in Table 2 suggest that the contribution of SAPO domains to both samples is considerably larger than that of AS domains. Therefore, the fact that the relative intensity ratio of the two prominent resonances appearing around −89 and −95 ppm decreases in the order SAPO-35(I) > SAPO-35(II) > SAPO-35(III) > SAPO-35(IV) further supports that the preference of Si atoms for the low-multiplicity site in SAPO-35 samples depends strongly on the extent of their substitution. This led us to believe that the Si substitution patterns in other structure types of SAPO molecular sieves with multiple T-sites, e.g., SAPO-11 (AEL), SAPO-18 (AEI), SAPO-40 (AFR), etc., would also be nonrandom, although some differences could exist when compared to the manner of Si substitution in SAPO-35. On the other hand, knowing the exact oxide composition of such domains created in SAPO molecular sieves is of fundamental interest, given the dependence of their Brønsted acidity on the extent of substitution of "nonisolated" Si atoms. It is generally believed that microporous SAPO materials with high Si contents have significant pure-silica island formation,[4b,17] mainly relying on $^{29}$Si MAS NMR results. However, this notion remains to be better defined, because there are also several published $^{29}$Si MAS NMR studies showing the generation of AS domains instead of silica islands at substitution levels even higher than the maximum limit of the isolated Si fraction in a particular SAPO framework.[18] Although the $^{29}$Si MAS NMR results in Figure 4 and Table 2 do not allow us to completely ascertain the absence of pure-silica islands in SAPO-35(IV), they strongly suggest that the generation of such islands in the SAPO-35 framework does not take precedence over the AS domain formation. This is not unexpected because the typical synthesis of SAPO molecular sieves includes the use of SAPO gels where the Si fraction is considerably low compared to the concentration of Al.

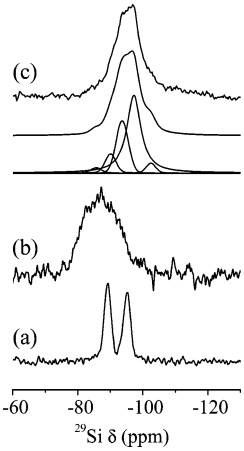


**Figure 5.** $^{29}$Si MAS NMR spectra of (a) as-made hydrated, (b) calcined hydrated, and (c) calcined dehydrated SAPO-35(II) samples. The traces given below the experimental spectrum of calcined dehydrated SAPO-35(II) are the simulated spectrum and its deconvoluted components, respectively.

Figure 5 shows the $^{29}$Si MAS NMR spectra of the hydrated and dehydrated forms of calcined SAPO-35(II). Unlike that of its as-made hydrated form, which is also given in Figure 5, the spectrum of calcined hydrated SAPO-35(II) exhibits a very broad resonance centered around −87 ppm. This appears to be mainly due to water molecules that strongly interact with the framework Si atoms. Table 1 shows that 8−9 water molecules per LEV cage are typically present in calcined hydrated SAPO-35 samples prepared here. The strong influence of adsorbed water on the $^{29}$Si MAS NMR spectrum can be further revealed when calcined hydrated SAPO-35(II) is dehydrated at 250 °C. As seen in Figure 5, the signal becomes narrow. However, notice that the $^{29}$Si MAS NMR spectrum of the calcined dehydrated sample is characterized by the line shape consisting of five deconvoluted components around −85, −90, −94, −97, and −103 ppm. Considering the chemical shifts of the two prominent $^{29}$Si resonances from its as-made hydrated form and their shift difference (6 ppm), as well as the possible changes in chemical shift caused by the removal of the occluded organic SDA, the two components appearing around −90 and −97 ppm can be tentatively assigned to $Si_1(4Al)$ and $Si_2(4Al)$ species in the SAPO region. Of particular interest is the observation that the relative intensity ratio (0.2:1) of these two components is much smaller than the value (1.1:1) calculated for as-made hydrated SAPO-35(II). This indicates that the extent of Si extraction from the SAPO-35 framework caused by calcination at 550 °C to remove the occluded organic SDA is much higher on the Si atoms in site $T_1$ than those in site $T_2$, like the case of Si substitution in the same framework. As described earlier, strain on $T_1$ is larger than on $T_2$, because the number of O−T−O bonds constrained within four rings is larger in the former than in the latter. Then, the preferential Si extraction from the high-multiplicity site during the calcinations step may be possible. In the case of some SAPO molecular sieves such as SAPO-37

**TABLE 3: $^{31}$P MAS NMR Data for As-Made SAPO-35 Materials Prepared Here**

| | $^{31}$P $\delta_{obs}$,[a] ppm from $H_3PO_4$ | | | | | | | | | | |
|---|---|---|---|---|---|---|---|---|---|---|---|
| | $P_A$ | | $P_B$ | | $P_C$ | | $P_1$(4Al) | | $P_2$(4Al) | | |
| sample | $\delta$ (ppm) | $I$ (%) | $\delta$ (ppm) | $I$ (%) | $\delta$ (ppm) | $I$ (%) | $\delta$ (ppm) | $I$ (%) | $\delta$ (ppm) | $I$ (%) | $I(P_1)/I(P_2)$ |
| SAPO-35(I) | −15.8 | 2.5 | −19.0 | 3.6 | −23.6 | 6.5 | −27.6 | 56.9 | −34.3 | 30.5 | 1.87 |
| SAPO-35(II) | | | | | −24.2 | 8.3 | −27.4 | 60.8 | −34.2 | 30.9 | 1.97 |
| SAPO-35(III) | | | | | | | −27.4 | 73.5 | −34.2 | 26.5 | 2.77 |
| SAPO-35(IV) | | | | | | | −27.7 | 68.0 | −34.0 | 32.0 | 2.13 |

[a] Observed chemical shifts from the deconvolution of the experimental spectra in Figure 6.

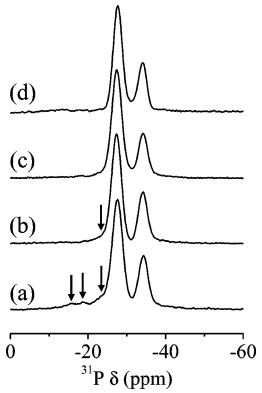


**Figure 6.** $^{31}$P MAS NMR spectra of as-made (a) SAPO-35(I), (b) SAPO-35(II), (c) SAPO-35(III), and (d) SAPO-35(IV).

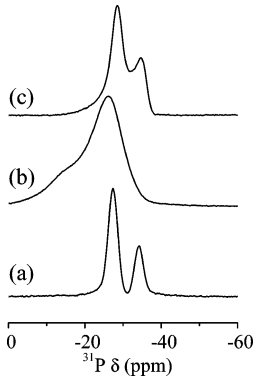


**Figure 7.** $^{31}$P MAS NMR spectra of (a) as-made SAPO-35(II) and its calcined form (b) before and (c) after dehydration under vacuum to a residual pressure of $10^{-3}$ Torr at 250 °C for 24 h.

(FAU) and ECR-40 (MEI),[19] on the other hand, it is claimed that reinsertion of some of the extracted Si atoms into the framework during the calcination at high temperatures can take place to form pure-silica islands, as well as AS domains. As seen in Figure 5, however, the calcined dehydrated SAPO-35 still shows a significant line broadening in the $^{29}$Si MAS NMR spectrum compared to its as-made hydrated form. Therefore, we cannot rule out the possibility that the appearance of three components around −86, −94, and −103 ppm in its $^{29}$Si MAS NMR spectrum could be attributed to the formation of an amorphous AS phase, although elucidating the details of their origin is beyond the scope of this paper.

Figure 6 shows the $^{31}$P MAS NMR spectra of the four as-made SAPO-35 samples studied here. All the samples exhibit two prominent $^{31}$P NMR resonances around −27 and −34 ppm, which is quite similar to the spectral feature reported in previous studies.[7a,20] As marked with arrows in Figure 6, however, the spectrum of SAPO-35(I) shows three additional low-intensity lines around −16, −19, and −24 ppm that are also observed for the corresponding sample obtained in a repeated synthesis run. These low-field resonances can be attributed to framework P atoms coordinated with water molecules and/or to those located at connectivity defects.[17c,21] The low-intensity shoulder around −24 ppm is also detected for SAPO-35(II), while none of these low-field lines exist for SAPO-35 samples with higher Si contents. When using the empirical correlation of Müller et al. between the $^{31}$P NMR chemical shifts and average P−O−Al angles in several nonmicroporous $AlPO_4$ phases,[22] the two tetrahedral $^{31}$P NMR resonances appearing around −27 and −34 ppm in Figure 6 can be assigned to $P_1$(4Al) in the D6R and $P_2$(4Al) in the S6R, respectively. The results from curve deconvolution of the $^{31}$P MAS NMR spectra in Figure 6 are given in Table 3. No linear relationship between the Si content of SAPO-35 samples prepared here and the relative intensity ratio of the two tetrahedral $^{31}$P NMR resonances was found, and this appears to be due to differences in their Si substitution pattern. It should be noted here that the relative intensity ratio (1.9:1) of the two tetrahedral $^{31}$P NMR resonances from SAPO-35(I) is slightly smaller that the value (2:1) calculated from the Si content of the corresponding sample and the relative intensity ratio (1.7:1) of its two tetrahedral $^{29}$Si NMR components. As given in Table 2, furthermore, a larger discrepancy between the intensity ratio (2:1) of the two tetrahedral $^{31}$P NMR resonances from SAPO-35(II) and the value (2.3:1) calculated in a way similar to that given above is observed. We speculate that this discrepancy may result from the coordination of some framework P atoms with water molecules which cause the intensity loss of tetrahedral $^{31}$P NMR resonances.

Figure 7 compares the $^{31}$P MAS NMR spectra of the hydrated and dehydrated forms of calcined SAPO-35(II) with the spectrum of its as-made hydrated form. Notice that a prominent $^{31}$P NMR resonance appearing around −34 ppm in the spectrum of as-made SAPO-35(II) due to $P_2$(4Al) in the S6R is completely missing in the spectrum of calcined hydrated SAPO-35(II). However, a new broad shoulder around −14 ppm, assignable to P atoms coordinated with water molecules,[21] is observed for the latter sample, which is also the case for the calcined, hydrated form of the other three SAPO-35 samples (Supporting Information Figure 3S). Therefore, we believe that the interactions of water molecules with T-atoms in the S6R are much stronger than those with T-atoms in the D6R, probably due to the relatively large average T−O−T angle for the low-multiplicity site compared to the high-multiplicity site. This can be further supported by the fact that the $^{31}$P NMR resonance around −34 ppm is almost regenerated by heating the calcined hydrated sample at 250 °C, as seen in Figure 7. However, curve deconvolution indicates that the relative intensity ratio (3.7:1) of the two tetrahedral $^{31}$P NMR resonances from calcined dehydrated SAPO-35(II) is considerably larger than the value (2:1) calculated for the calcined hydrated sample, confirming the strong effects of adsorbed water on the tetrahedral $^{31}$P MAS NMR resonances and hence giving the limited accuracy of their intensities. Finally, it should be noted that all the $^{27}$Al MAS NMR spectra of as-made SAPO-35 samples used here present a broad and complex line shape due to second-order quadrupolar interactions. Thus, no significant spectral changes were found

to arise from differences in the framework Si content of each sample (Supporting Information Figure 4S). Since this is also the case for the calcined hydrated samples, it appears that the $^{27}$Al MAS NMR data do not deliver additional information on the distribution of Si atoms in SAPO-35.

## Conclusions

We have demonstrated that substitution of Si atoms in two crystallographically distinct T-sites of the SAPO-35 framework is governed by the Si content in synthesis mixtures and their distribution over the two T-sites during crystallization occurs in a nonrandom manner. When the level of Si substitution in SAPO-35 materials is so high as to cause the heterogeneous distribution of Si atoms, the generation of aluminosilicate domains in the SAPO-35 crystals was found to take precedence over the pure-silica island formation. It is also shown that Si atoms are not randomly extracted from the SAPO-35 framework during the calcination step at elevated temperatures, because of differences in the expected strain on each T-site.

**Acknowledgment.** Support for this work was provided by the Korea Science and Engineering Foundation (R02-2003-000-10087-0) and the Carbon Dioxide Reduction and Sequestration Research Center (CB2-101-1-0-1), one of the 21st Century Frontier Programs funded by the Ministry of Science and Technology, Korea.

**Supporting Information Available:** Additional information as noted in the text. The material is available free of charge via the Internet at http://pubs.acs.org.

## References and Notes

(1) International Zeolite Association, Synthesis Commission, http://www.iza-synthesis.org.

(2) Han, O. H.; Kim, C.-S.; Hong, S. B. *Angew. Chem., Int. Ed.* **2002**, *41*, 469.

(3) Wilson, S. T.; Lok, B. M.; Messina, C. A.; Cannan, T. R.; Flanigen, E. M. *J. Am. Chem. Soc*. **1982**, *104*, 1146.

(4) (a) Lok, B. M.; Messina, C. A.; Patton, R. L.; Gajek, T. R.; Cannan, T. R.; Flanigen, E. M. *J. Am. Chem.* Soc. **1984**, *106*, 6092. (b) Flanigen, E. M.; Patton, R. L.; Wilson, S. T. *Stud. Surf. Sci. Catal*. **1988**, *37*, 13, and references therein.

(5) Hong, S. B.; Lee, S.-H.; Shin, C.-H.; Woo, A. J.; Alvarez, L. J.; Zicovich-Wilson, C. M.; Camblor, M. A. *J. Am. Chem. Soc*. **2004**, *126*, 13742, and references therein.

(6) International Zeolite Association, Structure Commission, http://www.iza-structure.org.

(7) (a) Prakash, A. M.; Hartmann, M.; Kevan, L. *Chem. Mater*. **1998**, *10*, 932. (b) Venkatathri, N.; Hedge, S. G.; Rajamohanan, P. R.; Sivasanker, S. *J. Chem. Soc., Faraday Trans*. **1997**, *93*, 3411.

(8) Altomare, A.; Burla, M. C.; Camalli, M.; Carrozzini, B.; Cascarano, G.; Giacovazzo, C.; Guagliardi, A.; Moliterini, A. G. G.; Polidori, G.; Rizzi, R. *J. Appl. Crystallogr*. **1998**, *32*, 339.

(9) (a) Dollish, F. R.; Fateley, W. G.; Bentley, F. F. *Characteristic Raman Frequencies of Organic Compounds*; Wiley: New York, 1974. (b) Lin-Vien, D.; Colthup, N. B.; Fateley, W. G.; Grasselli, J. G. *Handbook of* Infrared and Raman Characteristic Frequencies of Organic Molecules; Academic: San Diego, 1991.

(10) Bohlmann, F. *Angew. Chem.* **1957**, *69*, 641.

(11) Ramdas, S.; Klinowski, J. *Nature* **1984**, *308*, 521.

(12) McCusker, L. B. *Mater. Sci. Forum* **1993**, *133*−*136*, 423.

(13) (a) Abraham, A.; Lee, S.-H.; Shin, C.-H.; Hong, S. B.; Prins, R.; van Bokhoven, J. A. *Phys. Chem. Chem. Phys.* **2004**, *6*, 3031. (b) Han, B.; Lee, S.-H.; Shin, C.-H.; Cox, P. A.; Hong, S. B. *Chem. Mater*. **2005**, *17*, 477.

(14) Barthomeuf, D. *J. Phys. Chem.* **1993**, *97*, 10092.

(15) Engelhardt, G.; Michel, D. *High-Resolution Solid State NMR of Silicates and Zeolites*; Wiley: Chichester, 1987.

(16) Dupree, R.; Holland, D.; Williams, D. S. *Philos. Mag*. **1984**, *B50*, L13.

(17) (a) Martens, J. A.; Martens, M.; Grobet, P.; Jacobs, P. A. *Stud. Surf. Sci. Catal*. **1988**, *37*, 97. (b) Man, P. P.; Briend, M.; Peltre, M. J.; Lamy, A.; Beaunier, P.; Barthomeuf, D. *Zeolites* **1991**, *11*, 563. (c) Briend, M.; Peltre, M. J.; Lamy, A.; Man, P. P.; Barthomeuf, D. *J. Catal.* **1992**, *138*, 90.

(18) (a) Martens, J. A.; Janssens, C.; Grobet, P.; Jacobs, P. A. *Stud. Surf. Sci. Catal*. **1989**, *49A*, 215. (b) Maistriau, L.; Dumont, N.; Nagy, J. B.; Gabelica, Z.; Derouane, E. G. *Zeolites* **1990**, *10*, 243. (c) Martens, J. A.; Grobet, P.; Jacobs, P. A. *J. Catal.* **1990**, *126*, 299.

(19) (a) Derewinski, M.; Peltre, M. J.; Briend, M.; Barthomeuf, D.; Man, P. P. *J. Chem. Soc., Faraday Trans.* **1993**, *89*, 1823. (b) Afeworki, M.; Dorset, D. L.; Kennedy, G. J.; Strohmaier, K. G. In *Proceedings of the 14th International Zeolite Conference*; van Steen, E., Callanan, L. H., Claeys, M., Eds.; Document Transformation Technologies: Cape Town, 2004; pp 1274−1281.

(20) Blackwell, C. S.; Patton, R. L. *J. Phys. Chem.* **1988**, *92*, 3965.

(21) (a) Zubowa, H. L.; Alsdorf, E.; Fricke, R.; Neissendorfer, F.; Richter-Mendau, J.; Schreier, E.; Zeigan, D.; Zibrowius, B. *J. Chem. Soc., Faraday Trans*. **1990**, *86*, 2307. (b) Watanabe, Y.; Koiwai, A.; Takeuchi, H.; Hyodo, S. A.; Noda, S. *J. Catal.* **1993**, *143*, 430. (c) Buchholz, A.; Wang, W.; Arnold, A.; Xu, M.; Hunger, M. *Microporous Mesoporous Mater.* **2003**, *57*, 157.

(22) Müller, D.; Jahn, E.; Ladwig, G.; Haubenreisser, U. *Chem. Phys. Lett*. **1984**, *109*, 332.